AGU PUBLICATIONS

JGR

Journal of Geophysical Research: Atmospheres

RESEARCH ARTICLE
10.1002/2015JD024277

Key Points:
- Uncertainty in the photolysis rates related to SSI variability is characterized
- Ozone feedback can constitute up to a half of the stratospheric temperature response
- Performed analysis of photolysis codes is useful for CCM results interpretation

Correspondence to:
T. Sukhodolov,
timofei.sukhodolov@pmodwrc.ch

Citation:
Sukhodolov, T., et al. (2016), Evaluation of simulated photolysis rates and their response to solar irradiance variability, *J. Geophys. Res. Atmos.*, *121*, 6066–6084, doi:10.1002/2015JD024277.

Received 27 SEP 2015
Accepted 18 APR 2016
Accepted article online 20 APR 2016
Published online 21 MAY 2016

Evaluation of simulated photolysis rates and their response to solar irradiance variability

Timofei Sukhodolov[1,2], Eugene Rozanov[1,2], William T. Ball[1,2], Alkiviadis Bais[3], Kleareti Tourpali[3], Alexander I. Shapiro[4], Paul Telford[5], Sergey Smyshlyaev[6], Boris Fomin[7], Rolf Sander[8], Sébastien Bossay[9], Slimane Bekki[9], Marion Marchand[9], Martyn P. Chipperfield[10], Sandip Dhomse[10], Joanna D. Haigh[11], Thomas Peter[2], and Werner Schmutz[1]

[1]PMOD/WRC, Davos, Switzerland, [2]IAC ETH, Zurich, Switzerland, [3]LAP AUTh, Thessaloniki, Greece, [4]MPS, Göttingen, Germany, [5]NCAS Climate, University of Cambridge, Cambridge, UK, [6]RSHU, Saint Petersburg, Russia, [7]CAO, Moscow, Russia, [8]MPIC, Mainz, Germany, [9]LATMOS-IPSL, UVSQ, UPMC, Paris, France, [10]National Centre for Earth Observation, School of Earth and Environment, University of Leeds, Leeds, UK, [11]Grantham Institute, Imperial College London, London, UK

Abstract The state of the stratospheric ozone layer and the temperature structure of the atmosphere are largely controlled by the solar spectral irradiance (SSI) through its influence on heating and photolysis rates. This study focuses on the uncertainties in the photolysis rate response to solar irradiance variability related to the choice of SSI data set and to the performance of the photolysis codes used in global chemistry-climate models. To estimate the impact of SSI uncertainties, we compared several photolysis rates calculated with the radiative transfer model libRadtran, using SSI calculated with two models and observed during the Solar Radiation and Climate Experiment (SORCE) satellite mission. The importance of the calculated differences in the photolysis rate response for ozone and temperature changes has been estimated using 1-D a radiative-convective-photochemical model. We demonstrate that the main photolysis reactions, responsible for the solar signal in the stratosphere, are highly sensitive to the spectral distribution of SSI variations. Accordingly, the ozone changes and related ozone-temperature feedback are shown to depend substantially on the SSI data set being used, which highlights the necessity of obtaining accurate SSI variations. To evaluate the performance of photolysis codes, we compared the results of eight, widely used, photolysis codes against two reference schemes. We show that, in most cases, absolute values of the photolysis rates and their response to applied SSI changes agree within 30%. However, larger errors may appear in specific atmospheric regions because of differences, for instance, in the treatment of Rayleigh scattering, quantum yields, or absorption cross sections.

1. Introduction

There has been substantial progress in the study of the Sun's influence on climate and the ozone layer in recent years. Although several mechanisms based on observational analyses and model simulations have been proposed, not all of their aspects have been clearly identified [e.g., *Gray et al.*, 2010; *Ermolli et al.*, 2013; *Solanki et al.*, 2013]. The variability in the ultraviolet (UV) part of the solar spectrum is believed to affect the surface climate through the so-called "top-down" mechanism, which describes the dynamical coupling of the increased heating in the stratosphere during solar maximum with the local tropospheric decadal climate changes [*Kodera and Kuroda*, 2002; *Kidston et al.*, 2015]. The detection of this signal from the satellite observations is problematic due to the short data periods available. Chemistry-climate models (CCMs), which do not have such limitations, however, disagree even at the starting point of "top-down" mechanism—heating and ozone increase in the upper stratosphere by enhanced solar UV. The disagreement is related to the uncertainties in the solar forcing and its treatment by CCMs.

The main solar forcing mechanism is given by the spectral solar irradiance (SSI) changes. The magnitude and even the phase of SSI variations over the course of the activity cycle remain quite uncertain [*Ermolli et al.*, 2013; *Solanki et al.*, 2013; *Thuillier et al.*, 2014a, 2014b]. The most substantial difference between SSI data sets has come from the Solar Radiation and Climate Experiment (SORCE) satellite during the 23rd solar cycle (May 1996–January 2008). SORCE Spectral Irradiance Monitor (SIM) and Solar Stellar Irradiance Comparison Experiment (SOLSTICE) instruments revealed SSI variability in the UV up to 10 times larger than in all

previously measured and modeled data sets [*Harder et al.*, 2009; *Ermolli et al.*, 2013]. Results of CCM modeling studies, devoted to the uncertainty in SSI estimates, showed that the spectral distribution and magnitude of SSI changes define not only the amplitude but also the sign of the direct ozone response [*Oberländer et al.*, 2012; *Ermolli et al.*, 2013; *Shapiro et al.*, 2013].

However, even using the same SSI variability, different CCMs show a variety of results in amplitude and sign of stratospheric ozone and temperature responses [*Ermolli et al.*, 2013], indicating that there are differences between models in the representation of solar-induced stratospheric changes. The treatment of the solar signal in CCMs starts with the changes of the heating and photolysis rates, which are usually considered separately using different parameterizations. Essentially, the main part of the solar heating in the atmosphere also originates from the dissociation of the absorbing molecules (mostly O_3 and O_2) with subsequent recombination [*Mlynczak and Solomon*, 1993]. However, since recombination is fast at altitudes below the mesopause (~80 km), it was assumed in earlier climate models that the incoming solar energy is instantly converted into heat. At the same time, atmospheric chemistry transport models used prescribed temperature fields and considered solar energy only as a source of photodissociation [e.g., *Dhomse et al.*, 2011]. The integration of these two parts into CCMs has led to the existence of two separate sources of uncertainty in simulating the atmospheric response to solar irradiance variability. Our understanding of these two sources is not equal because uncertainties in heating rates and associated uncertainties in responses have been widely discussed in the literature [e.g., *Egorova et al.*, 2004; *Nissen et al.*, 2007; *SPARC CCMVal report*, 2010, Chapter 8; *Forster et al.*, 2011], whereas the response of photodissociation rates to solar variability has not yet been examined, except in some early studies [*Brasseur and Simon*, 1981], when the SSI changes were not well established.

The global ozone abundance depends on ozone production and destruction processes and transport by air motion. However, in the tropical stratosphere above ~30 km, the ozone concentration depends primarily on photochemical processes [e.g., *Brasseur and Solomon*, 2005]. In this region, ozone is produced mostly through the photolysis of molecular oxygen, followed by the recombination of atomic and molecular ozone in the presence of any third body molecule (M):

(R1) $$J_{O2} : O_2 + h\nu(\lambda < 242\ \text{nm}) \rightarrow O + O$$

(R2) $$O + O_2 + M \rightarrow O_3 + M.$$

The photolysis of ozone produces atomic oxygen

(R3) $$J_{O1D} : O_3 + h\nu(\lambda < 320\ \text{nm}) \rightarrow O(^1D) + O_2$$

(R4) $$J_{O3P} : O_3 + h\nu(\lambda < 850\ \text{nm}) \rightarrow O(^3P) + O_2,$$

which can then recombine back to ozone following (R2) or be consumed by source gases or radicals as a part of catalytic ozone destruction cycles. Radicals, which affect ozone, can be photolytically produced directly from source gases as in the following examples:

(R5) $$J_{CFC-11} : CFCl_3 + h\nu(170\ \text{nm} < \lambda < 240\ \text{nm}) \rightarrow 3Cl + \text{other products}$$

(R6) $$J_{H2O} : H_2O + h\nu(\lambda < 200\ \text{nm}) \rightarrow H + OH$$

and from reservoirs

(R7) $$J_{HNO3} : HNO_3 + h\nu(190\ \text{nm} < \lambda < 350\ \text{nm}) \rightarrow OH + NO_2$$

(R8) $$J_{ClONO2} : ClONO_2 + h\nu(200\ \text{nm} < \lambda < 400\ \text{nm}) \rightarrow Cl + NO_3$$

as well as indirectly

(R9) $$N_2O + O(^1D) \rightarrow NO + NO$$

(R10) $$H_2O + O(^1D) \rightarrow OH + OH.$$

In the stratosphere, photolysis of NO and NO_2 contributes positively to the ozone abundance. Photolysis of NO_2 slows down the NO_x catalytic cycle of ozone destruction through the production of atomic oxygen followed by the ozone production via (R2):

(R11) $$J_{NO2} : NO_2 + h\nu(230\ \text{nm} < \lambda < 650\ \text{nm}) \rightarrow NO + O,$$

while photolysis of NO initiates a main sink of odd nitrogen

(R12) $$J_{NO} : NO + h\nu(183\ \text{nm} < \lambda < 193\ \text{nm}) \rightarrow N + O$$

(R13) $$N + NO \rightarrow N_2 + O.$$

In the polar regions, the ozone depletion in late winter/early spring is also initiated by photolysis processes. One of the most important polar catalytic cycles of ozone destruction is the ClO dimer cycle described by *Molina and Molina* [1987]. Several studies [e.g., *Chipperfield et al.*, 2005; *von Hobe et al.*, 2007] showed that the uncertainties in Cl_2O_2 photolysis

(R14) $$J_{Cl2O2} : Cl_2O_2 + h\nu\ \ (200\ \text{nm} < \lambda < 450\ \text{nm}) \rightarrow 2Cl + O_2$$

can lead to large differences in the calculated ozone loss rate, since the formation of radicals defines the speed of ozone catalytic destruction cycles.

The precise solution of the radiative transfer equation (RTE) and the subsequent photolysis rate calculations are computationally too expensive for current CCMs; therefore, global models exploit simplified schemes or parameterizations. The disagreement between the different schemes can be caused by their spectral resolution, the method of solving the RTE, the treatment of the aerosols and clouds, and the applied values of absorption cross sections and quantum yields. Although recommended absorption cross sections and quantum yields are continuously updated [e.g., *Sander et al.*, 2011], not all models are kept up to date. Moreover, even with the same set of cross sections, uncertainties related to the method of wavelength integration, spectral resolution, or treatment of the temperature dependence cannot be excluded. Another source of uncertainty is the differences between the reference models used for the tuning of the parameterizations, which experience almost the same difficulties. All of these can lead to disagreement in the photolysis rates calculated with different parameterizations and, consequently, in the results of global models using these parameterizations. For example, *Hsu et al.* [2013] changed oxygen absorption cross sections in the Herzberg continuum (200–242 nm) by ±30% in a 3-D climate model with a coupled photochemistry module and found important implications for the stratospheric and tropospheric circulations. The "PhotoComp" section of CCMVal-2 report [*SPARC CCMVal*, 2010, Chapter 6] examined almost all recent photolysis parameterizations in various experiments. It showed that most of the parameterizations are in a reasonable agreement for 45 chemical constituents, although with a substantial spread for particular species and vertical levels. That comparison project avoided using one single code as a reference but performed comparisons with a "robust" mean, i.e., the mean calculated by excluding 2 sigma outliers. Such decision was motivated by a fact that there is not always a clear evidence of, e.g., which cross-section data to use or how to treat its temperature dependence. However, comparison with the mean made it difficult to properly define the specific features of each scheme, because even codes with different solar spectra could constitute the mean. The PhotoComp project also only focused on the absolute values of photolysis rates, and the response of each photolysis code to the SSI variability was not discussed, while the parameterization performance in this respect is important for modeling efforts aimed at Sun-Earth connections.

In this paper, we examine two major uncertainties related to the modeling of the solar irradiance influence on the photolysis rates: the choice of SSI data set and the performance of the photolysis codes frequently used in global chemistry-climate models. First, by performing the sensitivity experiments with 1-D radiative-convective-photochemical model (RCPM) [*Rozanov et al.*, 2002], we define which photolysis rates are the most important for ozone and temperature I the tropical stratosphere. Then, we address the questions of what are the solar variability-induced changes in the most important photolysis rates and how different they are for different SSI data sets. Further, we demonstrate the importance of the spectral resolution of the original SSI data sets for photolysis rate calculations. Finally, we analyze the performance of several state-of-the-art stratospheric photolysis parameterizations in terms of absolute values and response to solar variability by comparing their results to reference models using the latest recommended cross sections, quantum yields, and high-resolution SSI data.

2. Description of the Data Sets and Models

2.1. SSI Data Sets

We use SSI data obtained from two reconstructions and one composite based on SORCE observations [*Harder et al.*, 2009]. The SORCE composite consists of SOLSTICE v12 data below 310 nm and SIM v17 data for longer wavelengths and represents one of the highest level of the solar UV variability among published data sets. Although newer versions of SORCE data with different changes at different wavelengths have been released, here we use the version with one of the largest overall UV variability to illustrate the extreme case, which,

Table 1. Details of the SSI Data Sets Considered in This Study[a]

SSI Data Set	Timespan Used in the Study	Lyman-alpha line Variability, %	(A) 175–242 nm Variability, %	(B) 242–350 nm Variability, %	B/A
SORCE	6/2004–2/2009	20	3.64	0.99	0.29
NRL-part	6/2004–2/2009	15	1.20	0.11	0.09
NRL-full	4/2002–2/2009	46	3.73	0.33	0.09
COSI-part	6/2004–2/2009	18	1.31	0.25	0.22
COSI-full	4/2002–2/2009	55	3.35	0.75	0.22

[a]Variability is calculated as the change in % between active and quiet periods.

furthermore, has been widely used before in modeling studies [e.g., *Haigh et al*., 2010; *Ineson et al*., 2011; *Swartz et al*., 2013; *Ermolli et al*., 2013; *Shapiro et al*., 2013]. We also note that future releases may lead to further changes in the solar cycle trends, which, at least for the last three versions of SOLSTICE, lie within each other's uncertainties [*Ball et al*., 2014]. We also employ two theoretical reconstructions of solar irradiance: the Naval Research Laboratory (NRL) SSI reconstruction [*Lean*, 1997, 2000] and the reconstruction based on the Code for Solar Irradiance (COSI) [*Shapiro et al*., 2010] and described in *Shapiro et al*. [2011]. The NRL data set is chosen to represent the smallest solar UV variability and because it is the most frequently used data set in global climate models. The COSI reconstruction is used because it simulates the SSI variability in the 200–400 nm range closest to SORCE observations among all SSI data available [*Ermolli et al*., 2013], and also it provides SSI with very high spectral resolution.

The NRL reconstruction is based on the facular and sunspot contrasts calculated by *Solanki and Unruh* [1998] with ATLAS9 code [*Kurucz*, 1993]. Since the code is based on the assumption of the local thermodynamic equilibrium (LTE), which is not applicable in the UV, the data below 400 nm are based on the UARS/SOLSTICE measurements and multiple regression analysis. In contrast, COSI is a physics-based model of solar irradiance variability. It decomposes the solar disk into several magnetic components (quiet Sun, active network, faculae, and sunspots) and calculates solar irradiance by weighting the spectra of the individual components with corresponding disk area coverages [see *Shapiro et al*., 2011]. The code simultaneously solves the equations of radiative transfer and statistical equilibrium for all elements from hydrogen to zinc, which allows the code to properly calculate the spectra in the UV, where the assumption of the LTE breaks down. The COSI spectra and the absolute intensity returned by the code have been validated against numerous observed and theoretical spectra [*Shapiro et al*., 2010; *Ermolli et al*., 2013; *Thuillier et al*., 2014a, 2014b, 2015].

To study the effects of solar irradiance variability we use monthly averaged SSI from June 2004, an active time during the declining phase of cycle 23, and February 2009, near to the solar minimum. These months were selected because SORCE measurements do not cover the entire period of the solar cycle, so we take an early period in the data set to maximize the range we can investigate with SORCE. These dates reflect about one third of the sunspot number (SSN) change between a typical solar minimum and maximum (ΔSSN = 40.5). We also use the full cycle (ΔSSN = 120) from the COSI and NRL models to investigate how the uncertainty between two reconstructions can affect the photodissociation processes. The reconstruction data sets are referred here as COSI-full, COSI-part, NRL-full, and NRL-part. Technical information about the data sets is given in Table 1. The variability provided by each SSI data set was applied to the SORCE spectrum at solar minimum conditions to exclude the potential influence of the absolute spectrum differences, which has been shown to be important for the stratosphere [*Zhong et al*., 2008]. For the calculations performed here, we used the 120.5–700 nm spectral interval. For the analysis of the solar cycle, each of the SSI data was used with 1 nm sampling. The COSI data with higher sampling frequency are used for the analysis of the spectral resolution importance in section 5.1 and further for the comparison of the results from different photolysis parameterizations.

The relative difference of the SSI between active and quiet conditions (i.e., the variability) is shown in Figure 1 for the spectral range 180–370 nm. We show results for this spectral range because most CCMs have their top layer at around 80 km, below which wavelengths shorter than 180 nm, except the Lyman alpha line (121.6 nm), are not important. The variability in the Lyman alpha line integrated over 121–122 nm is presented in Table 1. Also, photolysis at wavelengths longer than 370 nm plays weaker role in the stratosphere-mesosphere region considered in this study. The agreement between reconstructions is rather good, showing a steady decrease of SSI variability with increasing wavelength. NRL shows higher variability than COSI in the 180–225 nm range, similar variability in the 225–240 nm range and lower variability at wavelengths longer than 240 nm. The magnitude of

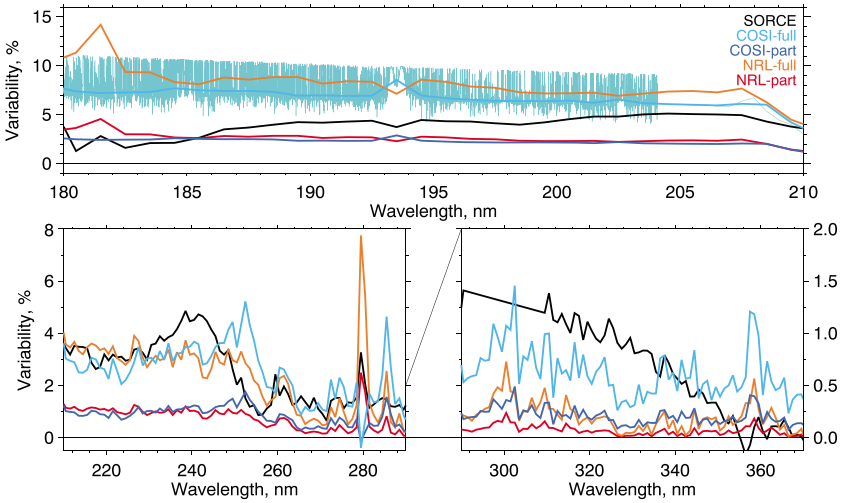

Figure 1. The relative difference (%) of the SSI between June 2004 and February 2009 for NRL-part, COSI-part, and SORCE data sets and the difference between solar maximum and minimum for NRL-full and COSI-full. All five data sets are plotted with a 1 nm sampling and are designated by colors given in the legend. The COSI-full data set is plotted, in addition, at a high resolution (light blue color). Different panels show different wavelength regions. Note the change of scale between the panels.

the SORCE SSI changes exceeds the model-based values by up to a factor 5, and in some regions, e.g., from 210 to 350 nm, it is comparable to, or even higher, than the magnitude of the reconstructed changes for the full cycle in NRL and COSI. The COSI data plotted with higher resolution illustrate the complicated structure of the Schuman-Runge bands (170–205 nm) consisting of many spectral lines.

2.2. Models of the Photolysis Rate Calculations

We have analyzed the performance of eight parameterizations against two reference models using an accurate solver of the RTE and very high spectral resolution. The details of these schemes are given in Table 2. As a reference, we used the high-resolution model *uvspec* of the LibRadtran package, a widely used tool for UV calculations that has demonstrated good accuracy in a number of validation campaigns [*Mayer and Kylling*, 2005]. LibRadtran was applied with a six-stream discrete ordinate solver in a spectrally resolved mode, specifically: 0.001 nm steps in the 121–130 nm range, 0.5 nm steps in the 130–175 nm range, 0.001–0.002 nm steps in the 175–205 nm range, 0.5 nm steps in the 205–305 nm range, and 1 nm steps in the 350–700 nm range. Another high-resolution model is the short-wave version of the FLBLM model [*Forster et al.*, 2011; *Fomin and Falaleeva*, 2012], which is based on the Monte Carlo approach and has a spectral resolution of 0.25 cm^{-1} (about 0.0004 nm at 125 nm and about 0.003 nm at 350 nm). Both reference models used linear interpolation and the latest recommended cross sections and quantum yields [*Sander et al.*, 2011] for all species except ozone (cross sections are mostly from *Molina and Molina* [1986] and quantum yields are from *Talukdar et al.* [1998]). The temperature dependence is taken into account with linear extrapolation beyond available ranges.

Table 2. Details of Photolysis Schemes Considered in This Study[a]

Scheme	Method and Version	Resolution	CS Comments	Lyman Alpha
SOCOL	LUT	73 bins [120–750 nm]	Mostly JPL17	Parameterized
FastJX	Online RT (v7.2)	18 bins [177–850 nm]	Mostly JPL17	None
TUV-LMDz	LUT	0.01–1 nm bins [116–850 nm]	Mostly JPL17	Parameterized
FastJX-UKCA	Online RT (v6.4)	Fast-JX + *Lary and Pyle* [1991] above 0.2 hPa	Mostly JPL15	Parameterized
JVAL	Partly LUT (v14)	8 bins [178.6–683 nm]	Mostly JPL17	Parameterized
SLIMCAT	LUT	158 bins [177–850 nm]	Mostly JPL17	Parameterized
SUNY-SPB	Online RT	78 bins [175–850 nm]	Mostly JPL17	None
HP	Online RT	171 bins [121–730 nm]	Diverse	Param. (no J_{H2O})
LibRadtran	Ref. code (v1.7)	0.001–1 nm bins	Mostly JPL17	Resolved
FLBLM	Ref. code	0.25 cm^{-1}	Mostly JPL17	Resolved

[a]LUT is a look-up table (or offline) approach to treat the radiative transfer (RT). JPL15 [*Sander et al.*, 2006] and JPL17 [*Sander et al.*, 2011] are the recommended rate data and cross sections based on laboratory measurements provided by Jet Propulsion Laboratory.

Part of the participating parameterizations is the schemes with an offline calculation of the radiative transfer (SOCOL based on *Rozanov et al*. [1999], JVAL [*Sander et al*., 2014], SLIMCAT/TOMCAT based on *Lary and Pyle* [1991], and TUV-LMDz [*Marchand et al*., 2012] based on TUV [*Madronich and Flocke*, 1999]). The idea of such schemes is that a model with a fine spectral resolution is used to create look-up tables (LUT), i.e., to precalculate photolysis rates and tabulate them as a function of several atmospheric parameters. Look-up tables are then used to obtain the photolysis rates by interpolation of the tabulated values to the current parameters given by a global model. This approach is widespread because of its high computational efficiency, since the most time consuming radiative transfer part is already solved offline or at infrequent intervals online. For example, the SLIMCAT model uses zonal mean fields to calculate a look-up table for each of the model latitudes every month in order to capture long-term solar variability and account for seasonal variations in ozone. However, the accuracy of the method largely depends on the number of parameters used for tabulation and their resolution, resulting in a large size of the stored look-up tables. The basic parameters defining the attenuation of the solar radiation are the O_3 and O_2 slant columns (along the light path), the temperature profile to account for the temperature dependence of the absorption cross sections, and pressure for the Rayleigh scattering. Usually, the cloud and aerosol effects, which are extremely important in the troposphere, are not considered for the calculations of LUTs and are added only to the already interpolated photolysis rates as modification coefficients. The JVAL scheme, however, in addition to precalculated photolysis rates in a pure absorbing atmosphere, performs the online calculation of influence of scattering by air molecules, aerosols, and cloud particles [*Landgraf and Crutzen*, 1998].

More accurate inclusion of all feedbacks related to the propagation of solar flux through the atmosphere recently became available with the development of radiative transfer schemes that are fast enough to be used online with global 3-D models. We consider here Fast-JX v7.2 [*Wild et al*., 2000; *Prather*, 2015] based on the eight-stream RTE solver and its modified version Fast-JX-UKCA based on Fast-JX v6.5 [*Telford et al*., 2013]. Schemes of this type have coarser spectral resolution but are validated against reference models. The accuracy of such schemes was also shown in the PhotoComp [*SPARC CCMVal report*, 2010, Chapter 6], where they all lie within 1 sigma uncertainty of the robust mean. The SUNY-SPB model [*Smyshlyaev et al*., 1998] and HP model [*Harwood and Pyle*, 1975] also use online schemes but only with the two-stream solver based on *Dvortsov et al*. [1992] and *Isaksen et al*. [1977], respectively.

We performed calculations with each of the participating schemes for each SSI data set using a tropical standard atmosphere with 42 vertical levels from 0 to 80 km [*McClatchey et al*., 1972], for aerosol and cloud-free conditions, for three solar zenith angles (10°, 40°, and 70°) and an albedo equal to 0.1. For the two high-resolution models (libRadtran and FLBLM) we applied exactly the same set of absorption cross sections, while for the parameterizations we kept the original settings, the details of which are given in Table 2. Therefore, the differences between the two reference models can be used as an estimate of the uncertainty in the parameterizations given by the reference models design, which is mostly due to resolution, RTE solution, and interpolation details.

2.3. One-Dimensional Radiative-Convective-Photochemistry Model (RCPM)

To illustrate the possible effect of the photolysis processes on ozone and temperature, we use a 1-D radiative-convective-photochemistry model (RCPM). The model was developed by *Egorova et al*. [1997] and *Rozanov et al*. [2002]. It consists of radiation, chemistry, convective adjustment, and vertical diffusion modules and has 40 layers from 0 km to 100 km. The photochemical part of the model calculates the distribution of 43 chemical species of the oxygen, nitrogen, hydrogen, carbon, chlorine, and bromine groups. To avoid any shortcomings of the model's original radiative transfer calculation scheme we apply all photolysis rate and heating rate changes related to SSI variations (sections 4.2 and 5.3) as scaling coefficients for the original RCPM photolysis and heating rate profiles, rather than directly apply SSI fluxes. Namely, we scale the internally generated photolysis and heating rate profiles using the relative changes calculated with libRadtran or other codes. We do the same, when we estimate the importance of the deviations of each code from libRadtran for the solar minimum conditions (sections 5.2 and 5.3). To reach the equilibrium state we then run the model in each experiment for 50 years with a 2 h time step and analyze the resulting ozone and temperature changes compared to the reference run. For all calculations we used a tropical standard atmosphere. As we use a 1-D model, which has no dynamical feedbacks, we do not consider its results as fully realistic but we use them only to illustrate the significance of different processes.

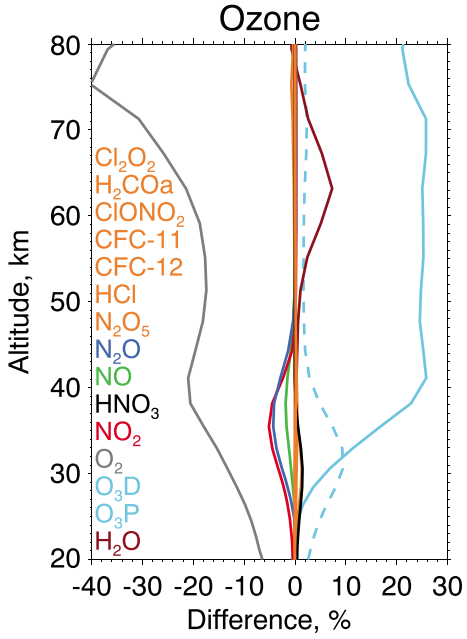

Figure 2. Response of ozone to the applied 30% decrease of photolysis rate profiles of different species simulated with RCPM. Different species are designated by different colors. Species with relatively small changes are plotted with the same orange color. Light blue solid and dashed lines show the contribution of $O(^1D)$ and $O(^3P)$ paths of ozone photolysis, respectively.

3. Ozone Sensitivity to Photolysis Rate Changes

In order to estimate the impact of photolysis rates from different species on ozone, we decreased J_{O2}, J_{O3P}, J_{O1D}, J_{H2O}, J_{Cl2O2}, J_{N2O}, J_{HNO3}, J_{NO2}, J_{NO}, $J_{CFC\text{-}11}$, $J_{CFC\text{-}12}$, J_{N2O5}, J_{ClONO2}, J_{H2COa}, and J_{HCl} in the RCPM separately by 30% over the entire model vertical profile. Experiments with other changes (±10%, ±20%, and +30%) showed that the RCPM ozone response to changes up to at least 30% is linear. Therefore, we used −30% for illustration here because most of photolysis deviations, revealed by the PhotoComp project [*SPARC CCMVal* report, 2010, Chapter 6], were within ±30%, and thus, our results can be compared with that study. The comparison of these results to the unperturbed model run is presented in Figure 2. Our results show that the most important contributors to ozone burden in the tropical stratosphere and mesosphere are production through J_{O2} and destruction involving J_{O3P} and J_{O1D}. In addition to the direct destruction, J_{O1D} also contributes to the ozone destruction via (R9) and (R10). In the mesosphere, photolysis of water vapor also plays a substantial role through the production of HO_x radicals.

The ozone response to the photolysis of other species is much smaller. The most pronounced effects are the middle-stratospheric negative ozone reactions to the decrease of J_{N2O}, J_{NO2}, and J_{NO}. The N_2O photolysis is a minor source of $O(^1D)$, which then can contribute either to ozone destruction via (R9) and (R10) or to ozone production via R2 after quenching to the ground level by collision with N_2 or O_2. The NO_2 photolysis partly compensates the ozone destruction by NO in the middle stratosphere. The expected effect from SSI variability should be much smaller, since NO_2 absorbs mostly in the near UV; however, J_{NO2} is highly dependent on Rayleigh scattering, which is a weak side of some photolysis codes. Photolysis of NO determines the main reactive nitrogen sink. J_{NO} is additionally important as it had the largest uncertainty in PhotoComp [*SPARC CCMVal report*, 2010, Chapter 6]. This is related to the fact that the precise calculation of J_{NO} is complicated and requires a detailed knowledge of the solar spectrum and O_2 and NO absorption cross sections. Modeling groups therefore use different empirical approximations, which are even not covered by IUPAC [*Atkinson et al*., 2004] or JPL [*Sander et al*., 2006, 2011] recommendations. The ozone decrease due to the reduction in the photolysis of reservoir species $ClONO_2$, HCl, and HNO_3 is rather small.

4. The Response of the Photolysis Rates to SSI Changes and Their Uncertainty

4.1. The Response of the Photolysis Rates to SSI Changes

Following from the results of section 3, to investigate the solar signal response we focus on the most important photolysis reactions for ozone, namely, the photolysis of O_2, O_3 (both $J_{O1D} + J_{O3P}$), and H_2O. We also analyze the photolysis of HNO_3 and NO_2, in order to investigate the solar variability-induced changes and parameterization performance for species absorbing in different UV spectral regions (190–300 nm and 300–400 nm, respectively), and the photolysis of Cl_2O_2—the crucial reaction for the polar ozone chemistry. The photodissociation rate J of molecule A can be expressed by the equation

$$J_A = \int_{\lambda_1}^{\lambda_2} \sigma_A(\lambda, T) q_A(\lambda, T) I(\lambda) \mathrm{d}\lambda, \quad (1)$$

where σ_A and q_A are the wavelength (λ) and temperature (T) dependent absorption cross sections and quantum yields of gas A and $I(\lambda)$ is the actinic flux. λ_1-λ_2 is the part of the solar spectrum over which

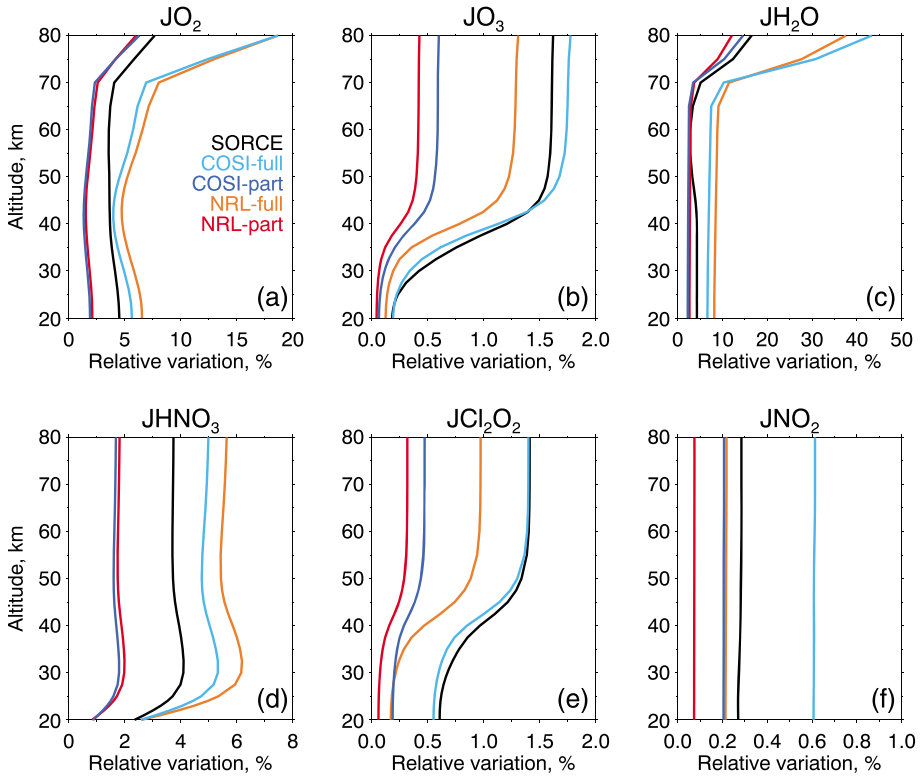

Figure 3. The relative difference (%) in the photolysis rates calculated by libRadtran using the NRL-part, COSI-part, and SORCE data sets between June 2004 (medium solar activity) and February 2009 (near solar minimum) and NRL-full and COSI-full between solar maximum and minimum. Calculations are performed for a tropical atmosphere, with a solar zenith angle equal to 10° and an albedo of 0.1. Note the different *x* axis scale for each panel.

the molecule can dissociate. Following equation (1), the magnitude of the photolysis rate response represents the combination of the spectral distributions of the SSI, the SSI variability, and the absorption cross sections and quantum yields. The changes in the photolysis rates from February 2009 to June 2004 for the SORCE, NRL-part and COSI-part data sets and the full solar cycle differences for the COSI-full and NRL-full data sets calculated by the libRadtran are shown in Figure 3. The changes are presented as a relative difference between the photolysis rate during the solar minimum $J_{A,\ \mathrm{min}}$ and the photolysis rate during the solar maximum $J_{A,\ \mathrm{max}}$:

$$\Delta J_A = \frac{\left(J_{A,\ \mathrm{max}} - J_{A,\ \mathrm{min}}\right)}{J_{A,\ \mathrm{min}}} \times 100. \tag{2}$$

In the middle stratosphere, oxygen photolysis occurs mostly in the Herzberg continuum (200–242 nm), where the weak oxygen absorption allows solar flux to penetrate down into the lower stratosphere. In the upper stratosphere and mesosphere, oxygen photolysis in the Lyman alpha line and Schumann-Runge bands is more important. The Schumann-Runge continuum (135–176 nm) is only important above 90 km due to its strong absorption. In Figure 3a, the largest changes, up to 15 % for the full cycle and 5% for the 2004–2009 period, are found in the mesosphere following the high SSI variability in the Lyman alpha line and Schumann-Runge bands. At the altitudes of maximum ozone abundance in the middle stratosphere, variability of oxygen photolysis rates is about 3 times smaller and is dominated mainly by the Herzberg continuum. NRL results are slightly larger than COSI because of higher variability in NRL in 180–230 nm range. SORCE results are very close to the COSI full in the stratosphere because of the similar SSI variability in the Herzberg continuum. However, they have a straighter vertical profile due to the variability behavior in the Schuman-Runge bands, which is different to NRL and COSI and decreases at shorter wavelengths.

Ozone photolysis in the 20–80 km layer is determined mostly by the ozone absorption in the Hartley (200–300 nm), Huggins (320–360 nm), and Chappuis (375–650 nm) bands [e.g., *Brasseur and Solomon*, 2005]. In Figure 3b, large and homogeneous photolysis rate changes are calculated in the upper layers (50–80 km) because the ozone absorption is rather weak there, and the SSI variability is larger for the shorter wavelengths. Starting from 50 km, the absorption of solar irradiance by ozone leads to a reduction in the short, highly variable, UV wavelengths, leading to a less intensive response of the photolysis rates at lower altitudes due to the smaller variability of the SSI at longer wavelengths. This feature is even more pronounced for larger solar zenith angles (not shown) due to the increase of optical paths and larger absorption by ozone. The magnitude of the photolysis rate response depends directly on the SSI changes in the considered wavelength interval. Therefore, the ozone photolysis increases only marginally (less than 0.6%) for NRL-part and COSI-part reconstructions with a slightly larger magnitude for the COSI data set. The J_{O3} changes for the SORCE data set are larger even than for NRL-full along the whole profile and larger than for COSI-full below ~45 km, because SORCE has higher variability at wavelengths that dominate the ozone photolysis response in the stratosphere, i.e., the Hartley and Huggins bands.

Photolysis of H_2O in the stratosphere and mesosphere is dominated by the Lyman alpha line. This explains the small difference between the three SSI data sets considering the 2004–2009 period, since the Lyman alpha irradiance is similar for all considered SSI data sets (Table 1). This reaction is highly sensitive to solar variations and is important for the simulation of the influence of the 27 day and 11 year solar irradiance variability on the tropical mesospheric ozone and water vapor, as shown in many observational and modeling studies [e.g., *Rozanov et al*., 2006; *Shapiro et al*., 2012].

Since NO_2 photolysis mostly occurs in the ~300–400 nm range, all differences between the SSI data sets, shown in Figure 3f, can be explained by changes in this spectral interval. All changes have a flat vertical pattern and do not exceed a few tenths of a percent. Cl_2O_2 and HNO_3 are reservoir species that bind ozone-destroying radicals and release them through daytime photolysis. Both species play a significant role in polar ozone-related heterogeneous chemistry. Variations of SSI in the 190–300 nm and 200–450 nm spectral ranges explain the results in Figures 3d and 3e calculated for HNO_3 and Cl_2O_2, respectively.

4.2. Effects of SSI Uncertainty on Ozone and Temperature

To illustrate the importance of the differences obtained between SSI data sets we use RCPM to calculate ozone and temperature responses to the changes in the oxygen, ozone, and water vapor photolysis analyzed in section 4.1 (JR case, Figures 4a and 4b). Since the heating also depends directly on the SSI variations and can compensate or enhance the photolysis effects, we also performed calculations with the corrected heating rate profiles (HR case, Figures 4c and 4d) and with heating rate and three photolysis rate profiles corrected together (HR + JR case, Figures 4e and 4f). All the applied perturbations of heating and photolysis rates were calculated using the libRadtran model. The results are presented as a difference between the unperturbed and experiment runs driven by the changes of the SSI from all considered data sets. The temperature response to the SORCE SSI changes is 1.5–2 times larger over the entire model domain than the response to NRL-part and COSI-part, which are quite similar, and even larger than NRL-full and COSI-full below ~45 km (Figure 4f). The ozone response is about 2 times larger for SORCE than for NRL-part and COSI-part below 35 km due to stronger oxygen photolysis in the Herzberg continuum (Figure 4e). The negative ozone response around the stratopause (50–65 km) for SORCE is due to the high SSI variability in the ozone Hartley and Huggins bands, which provides more ozone destruction both due to the increased ozone photolysis and to the enhanced temperature. The differences between ozone response to NRL and COSI SSI variations maximize between 35 and 65 km. The 65–80 km region, which is dominated by the Lyman alpha line and Schumann-Runge bands irradiance, shows similar ozone response for all three data sets.

Interestingly, although the COSI-full and NRL-full SSI variability differences are smaller than those of SORCE and NRL-part, the wavelength distribution of these differences leads to an ozone response difference of similar, or even higher, magnitude at particular altitudes (30–65 km, Figure 4e). On one hand, this means that SSI data sets even with less UV variability as given by SORCE can provide sufficiently different ozone responses qualitatively and quantitatively. On the other hand, the ozone-to-temperature feedback difference (JR case) between NRL-full and COSI-full is compensated by the difference in the heating rate response (HR case) and the overall effect on temperature is similar for both data sets (HR + JR case, Figure 4f).

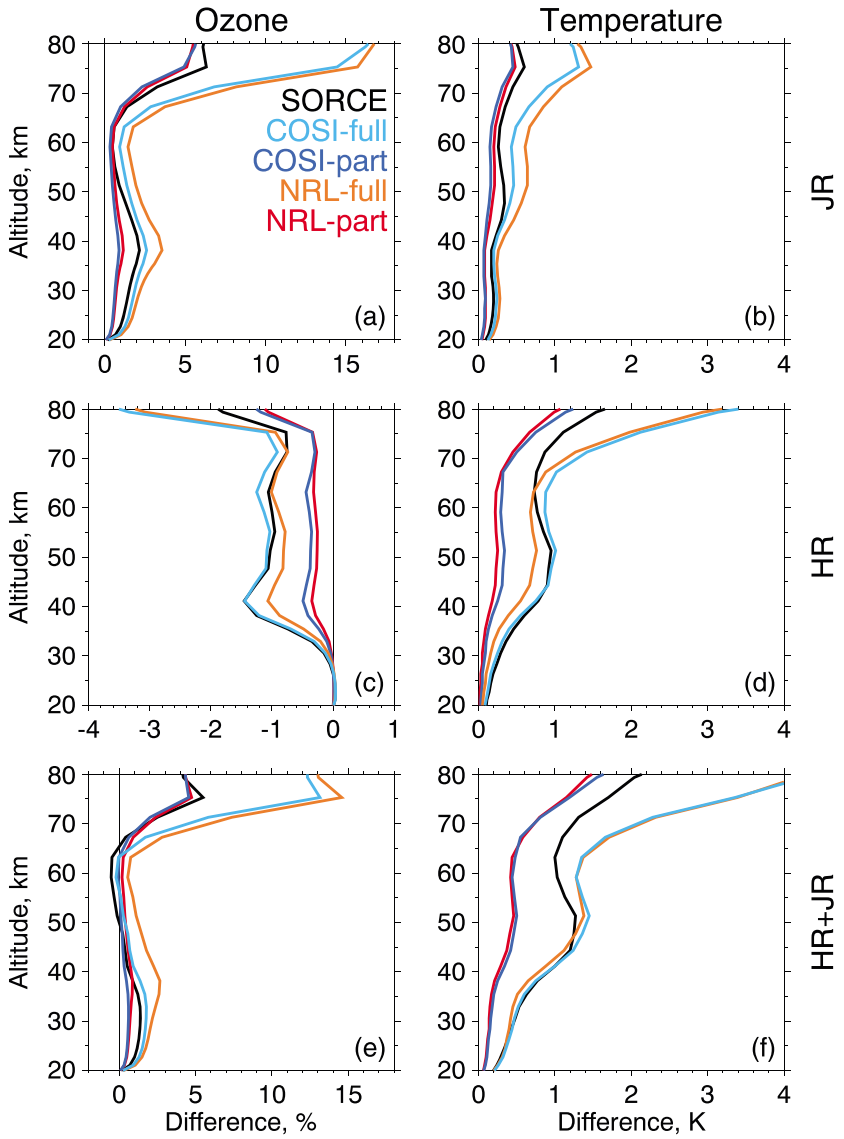

Figure 4. Response of (a, c, and e) ozone and (b, d, and f) temperature profiles to the applied corrections of photolysis profiles of oxygen, ozone, and water vapor (JR), to the correction of heating rates (HR) and to the heating rates and three photolysis rates correction together (HR + JR) simulated with RCPM. Correction factors are calculated from the results of Figure 3. Different SSI data sets are designated by different colors. Note the different *x* axis scales Figures 4a, 4c, and 4e.

Our results therefore confirm the high importance of the spectral distribution of SSI variations on the atmosphere as previously mentioned by several studies [e.g., *Haigh*, 1994; *Rozanov et al.*, 2002; *Ermolli et al.*, 2013; *Swartz et al.*, 2013; *Ball et al.*, 2016]. As presented schematically in Figure 5, temperature and ozone changes balance each other. SSI variations introduce imbalance to the system through the changing of photolysis and heating rates. Both oxygen and ozone absorption contribute to the heating rate increase and the following negative feedback on ozone, but their photolytic effect differs, and as shown in Figure 2, the increase of oxygen photolysis always leads to additional ozone production while the increase of ozone photolysis always enhances ozone destruction. Therefore, in the stratosphere the difference between SSI data sets due to the interaction between these main processes can be represented as a ratio between the SSI variations in the main ozone absorbing wavelengths (242–350 nm) and oxygen absorbing wavelengths (175–242 nm). Ozone also absorbs in the 200–242 nm band, but the overall effect on ozone of this spectral interval is positive. Since the Lyman alpha variations do not differ substantially among data sets we do not discuss them here. These ratios are presented in

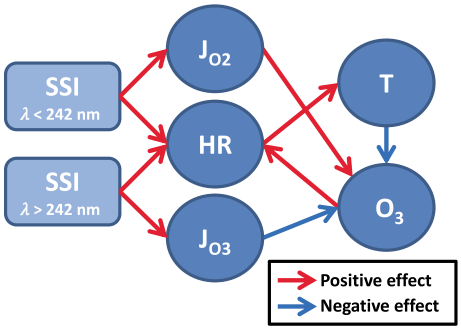

Figure 5. The feedback chain initiated by an increase in spectral solar irradiance (SSI) at wavelength regions shorter and longer than 242 nm typical for the tropical middle stratosphere. Enhanced SSI leads to the increase in heating rates (HR) and ozone and oxygen photolysis (J_{O3} and J_{O2}). The heating rate increase together with the ozone (O_3) increase due to increased oxygen photolysis lead to a higher temperature (T), which is partly compensated by the additional ozone destruction due to increased ozone photolysis and temperature feedback, namely, the acceleration of the temperature-dependent ozone-destroying catalytic cycles.

Table 1. From these we can conclude that the higher the ratio the more the ozone response is shifted toward the negative in the upper stratosphere/lower mesosphere, and the less the fraction of the temperature response is determined by the photolysis effect. Thus, the contribution to the temperature response for the SORCE and COSI data sets is ~1.5–2.5 times higher for the heating rates (Figure 4d) than for the photolysis rates (Figure 4b) everywhere except the lowermost stratosphere, where the temperature increase due to the additional ozone, produced through the oxygen photolysis in Herzberg continuum, becomes more important. While in the case of NRL-part the contribution of the photolysis and heating effects is of similar importance. Note that our results are fully photochemical, while for the lower stratosphere the importance of dynamical feedbacks is increasing. *Swartz et al.* [2013] found qualitatively similar results of photolysis and heating rate separation also for the polar regions using 2-D and 3-D CCMs.

5. Uncertainty in Photolysis Rate Modeling

5.1. Effects Caused by the Spectral Resolution

SSI data measured by satellites or calculated by SSI models are usually provided to users with a 1 nm sampling. It is generally accepted that 1 nm spectral resolution is sufficient to fully resolve any spectral variation in the broad ozone absorption Hartley, Huggins, and Chappuis bands. However, the oxygen absorption in the Schuman-Runge bands, which is an important source of $O(^3P)$, is a complex system and requires a higher resolution to properly describe the solar and absorption spectra. The solar hydrogen emission Lyman alpha line is also an important source of dissociation for oxygen, water vapor, and other chemical constituents, because it is so strong that the irradiance penetrates down to the mesosphere. The problem is that the shape of the line is complicated, and so application of the mean irradiance and/or cross sections will lead to some errors in the vertical profile of photolysis rates.

To understand the importance of the SSI data resolution we calculated the oxygen photolysis rates using our reference model libRadtran with the original COSI-full data set, which resolves the Schumann-Runge bands and the Lyman alpha line, and with the COSI-full data set with the spectral resolution decreased to 0.5 and 1 nm. The results of these two experiments relative to the case with original high resolution are presented in Figure 6 for solar minimum conditions (a)

$$\Delta J_A = \frac{\left(J_{A,\ \mathrm{mod}} - J_{A,\ \mathrm{ref}}\right)}{J_{A,\ \mathrm{ref}}} \times 100 \tag{3}$$

and for the solar signal (b)

$$\Delta J_A = \frac{\left(\Delta J_{A,\ \mathrm{mod}} - \Delta J_{A,\ \mathrm{ref}}\right)}{\Delta J_{A,\ \mathrm{ref}}} \times 100, \tag{4}$$

where A is oxygen, and $J_{A,\ \mathrm{ref}}$ and $J_{A,\ \mathrm{mod}}$ are the photolysis rates under solar minimum conditions in the high-resolution reference case and one of the cases with the decreased resolution, respectively. $\Delta J_{A,\ \mathrm{ref}}$ and $\Delta J_{A,\ \mathrm{mod}}$ are the same but for the solar signal (maximum–mininum). For the solar minimum conditions the J_{O2} deviations can be as high as 19% in the mesosphere and 5–10% in the stratosphere. The solar signal deviations also maximize in the mesosphere up to 36% and are rather small in the stratosphere—less than 3%. The deviations are both positive and negative and are higher for 1 nm than for 0.5 nm spectral resolutions. The effects are not directly connected to the performance of parameterizations used in climate models, because their resolution

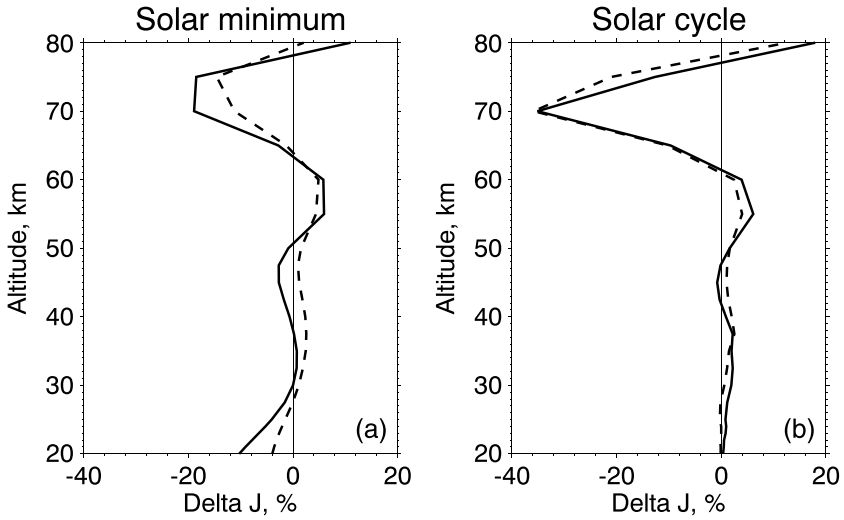

Figure 6. Differences in the oxygen photolysis rates calculated by libRadtran using the COSI-full SSI data set with a 1 nm (solid line) and 0.5 nm (dashed line) spectral resolution relative to the case using the original COSI-full high spectral resolution with the resolved Schuman-Runge bands and Lyman alpha line. Calculations are performed for a tropical atmosphere, solar zenith angle equal to 10°, and albedo of 0.1.

is generally poorer than 1 nm. However, the higher-resolution codes that were used to tune the parameterizations could employ the solar spectrum and oxygen cross sections with a coarse resolution and thereby transmit the error to the parameterizations. The performance of photolysis parameterizations is the second main source of uncertainty for the modeled solar signal and determines not only the direct response of chemistry to the solar changes but also the average state of chemical composition, notably the ozone distribution, and thus the response to any other perturbation including the thermal effects of solar changes.

5.2. Analysis of the Performance of Parameterizations for the Solar Minimum Conditions

A comparison of photolysis rates calculated by eight parameterizations and two high spectral resolution codes relative to libRadtran is presented in Figure 7. This is also based on equation (3) but for different species and $J_{A,\,\mathrm{ref}}$ being libRadtran and $J_{A,\,\mathrm{mod}}$ being the result of each parameterization. We used the COSI data set at solar minimum conditions, a solar zenith angle of 10°, and an albedo of 0.1. The agreement between the high-resolution models libRadtran and FLBLM is good and the differences generally do not exceed 5% for all chemical species considered, except for H_2O in the stratosphere, where J_{H2O} values are very small and are not crucially important for the chemistry. Since these two models used the same sources for absorption cross sections, the differences may originate from the RTE solvers and the spectral resolutions of the models. Additional tests (not shown) revealed that even the choice of the SSI interpolation method can result in clear differences, particularly in the Schumann-Runge bands and the Lyman alpha line.

The Fast-JX code uses an online solution of the radiative transfer and has 18 wavelength bins, between 177 and 850 nm [*Bian and Prather*, 2002]. Because Fast-JX does not provide photolysis rates for wavelengths below 177 nm, which are important for some reactions in the upper stratosphere and mesosphere (e.g., (R1) and (R6)), it was upgraded by *Telford et al.* [2013] for the UKCA component of the MetUM CCM. They calculated photolysis rates for these wavelengths using the offline scheme from *Lary and Pyle* [1991] with the Lyman alpha parameterization based on *Nicolet* [1985] and added them to the Fast-JX reaction rates above 0.2 hPa. In Figure 7, this addition is manifested as the increase of J_{O2} in the mesosphere and the inclusion of the J_{H2O} reaction, which was absent in Fast-JX. All other differences between Fast-JX and Fast-JX-UKCA results originate mostly from absorption cross sections differences and can be as high as tens of a percent. This example is an illustration of the uncertainty caused by the absorption cross sections, which are not always the same in atmospheric chemistry modeling studies, especially if one compares present-day studies with earlier ones. Fast-JX exploits cross sections that are more up-to-date and shows better agreement with libRadtran and FLBLM compared to Fast-JX-UKCA. Another two schemes with an online solution of the RTE, SUNY-SPB and HP, shows

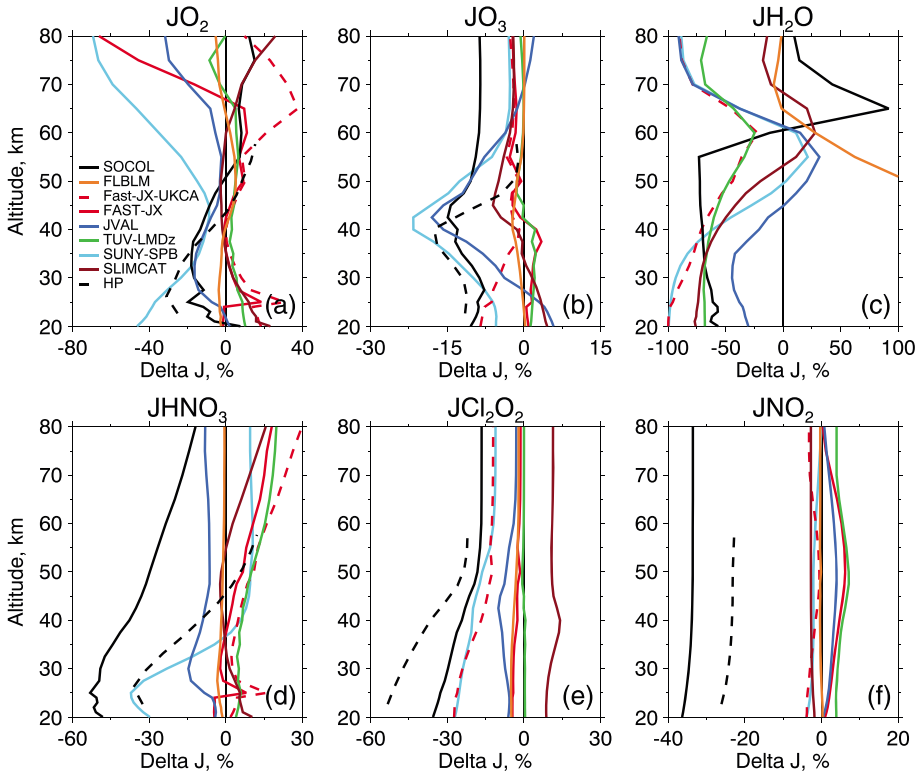

Figure 7. The relative difference (%) between the photolysis rates calculated by libRadtran and other codes using the COSI SSI data set for solar minimum conditions, tropical atmosphere, solar zenith angle equal to 10°, and albedo of 0.1.

certain problems in reproducing stratospheric values, which can be related to the Rayleigh scattering treatment. Look-up table (LUT)-based schemes (SOCOL, TUV, SLIMCAT, and JVAL) show a large variety of results. The lowest deviations (5–10%) between these schemes compared to libRadtran are shown by TUV-LMDz, except cases related to Lyman alpha, and SLIMCAT, for all species except Cl_2O_2. The large SLIMCAT J_{Cl2O2} values are due to the model using a long wavelength extrapolation of the JPL data set in order to reproduce observed polar ozone loss rates [see *Chipperfield et al.*, 2005]. Interestingly, the SLIMCAT look-up table code, which is an extensively updated version based on *Lary and Pyle* [1991], shows much better agreement with the reference codes for mesospheric J_{O2} and J_{H2O}. This is in contrast to Fast-JX-UKCA, which also uses a scheme based on *Lary and Pyle* [1991], but with different modifications, for the wavelengths below 177 nm. The deviations of the SOCOL scheme in the stratosphere are largely defined by the neglected Rayleigh scattering effect and temperature dependence of absorption cross sections and quantum yields. These results are mainly consistent with the PhotoComp project [*SPARC CCMVal report*, 2010, Chapter 6]. Generally, schemes, which directly apply the two-stream scattering approach (SUNY-SPB, HP) or in a form of LUTs but calculated by two-stream higher-resolution codes (SOCOL, partly JVAL), are similar to each other and show worse results in the lower stratosphere than the schemes which apply multistream scattering (Fast-JX, Fast-JX-UKCA, SLIMCAT, and TUV-LMDz). *Olson et al.* [1997] made the same conclusion examining results of a number of photolysis codes in the troposphere, where the effect of Rayleigh scattering is larger.

To evaluate the possible effects of parameterizations inaccuracies we performed RCPM experiments similar to the previous sections but with the J_{O2}, J_{O3} and J_{H2O} correction factors calculated from the deviation of the codes from libRadtran. The results are presented in Figure 8 and should be understood as the possible effects on the climatological results of CCMs caused by photolysis parameterizations. The effects are higher in the mesosphere because of the parameterizations uncertainty in J_{O2} and J_{H2O} related to the Lyman alpha line and Schumann-Runge bands. Note that the parameterizations shortcomings related to different species can offset or strengthen each other's effects on ozone. Thus, for example, SOCOL's ozone overestimation in the mesosphere due to overestimated J_{O2} is compensated partly by the effect of overestimated J_{H2O}, or underestimated J_{O3} and

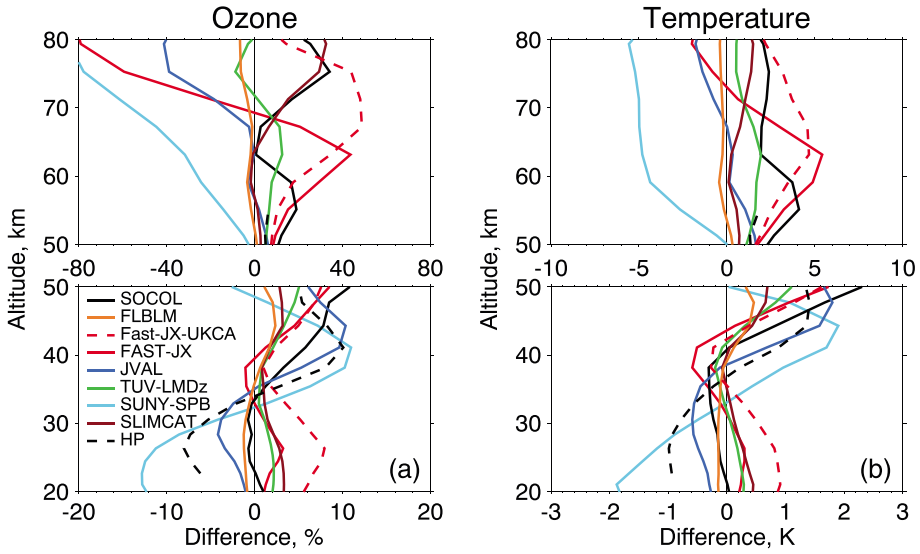

Figure 8. Response of ozone and temperature profiles to the applied corrections of J_{O2}, J_{O3}, and J_{H2O} simulated with RCPM. Correction factors are calculated from the behavior of parameterizations in Figure 7.

overestimated J_{O2} in Fast-JX-UKCA deviations in the lower stratosphere amplify each other and result in ozone overestimation. The resulting stratospheric temperature changes then can indirectly affect the troposphere [*Haigh*, 1996; *Kodera and Kuroda*, 2002; *Hsu et al.*, 2013]. The results presented can be used to understand the CCMs behavior in comparison with observations. Direct photolysis effects are always overlapped with other chemical and dynamical processes; therefore, our modeling results should be used to define the sign and the

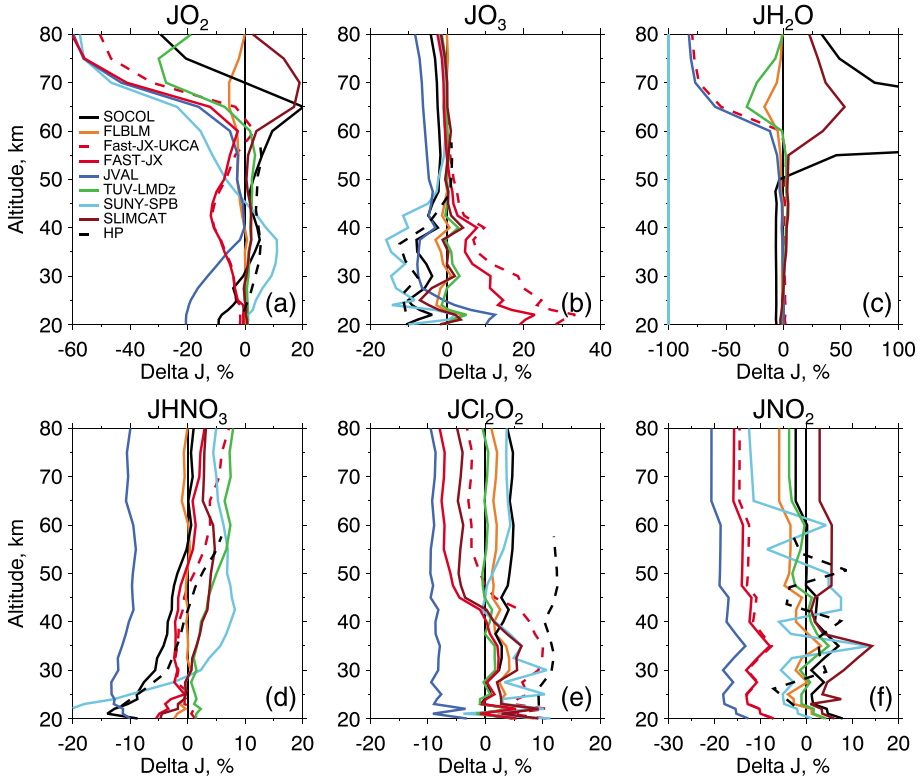

Figure 9. The relative difference (%) between the solar signal (maximum–minimum) from photolysis rates calculated by libRadtran and other codes using the COSI-full SSI data set, a tropical atmosphere, a solar zenith angle equal to 10°, and an albedo equal to 0.1.

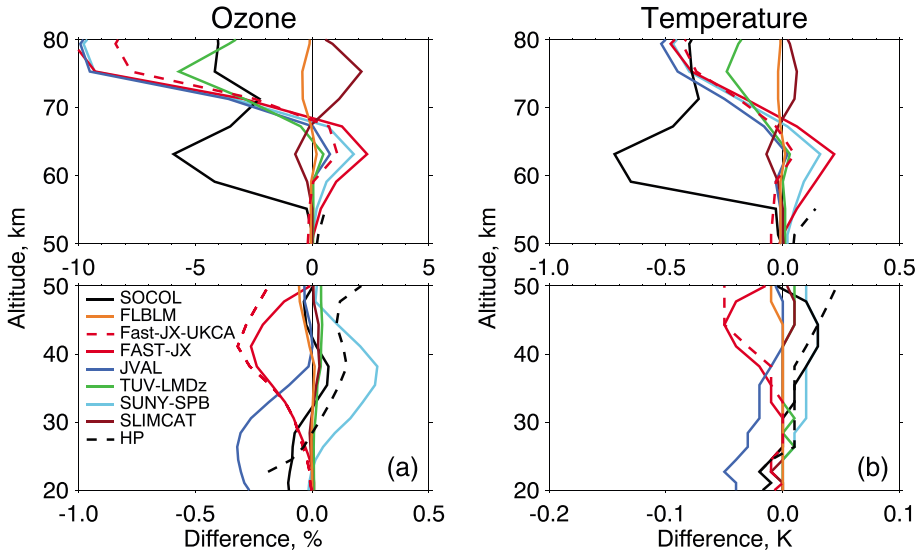

Figure 10. The difference between the solar signals in 1-D-modeled ozone and temperature due to corrected profiles of J_{O2}, J_{O3}, and J_{H2O} using different parameterizations and libRadtran (Figure 4, JR COSI-full case).

relative strength of the deviation and not as an exact estimate, especially in the lower stratosphere, where the dynamics plays a larger role. For example, we show that the SOCOL CCM is expected to overestimate average ozone and temperature in the upper stratosphere and mesosphere, which is qualitatively consistent with the SOCOL CCM tropical ozone and temperature behavior compared to observations [*Stenke et al*., 2013]. Note also that we applied only the changes of J_{O2}, J_{O3}, and J_{H2O}, while large errors in photolysis of other species can become important for certain altitudes (e.g., J_{NO} in the middle stratosphere).

5.3. Analysis of the Performance of Parameterizations for the Solar Signal

Figure 9 shows the parameterizations performance in reproducing the photolysis rate response to solar variability, i.e., the relative difference between the solar signals calculated by the participating schemes and libRadtran, which is similar to equation (4) but $\Delta J_{A,\,ref}$ being the libRadtran results and $\Delta J_{A,\,mod}$—the results of each scheme. Again, we used here the COSI-full data set, solar zenith angle equal to 10°, and an albedo equal to 0.1. The results should be interpreted as a part of the solar signal underestimated or overestimated by parameterizations. The high spectral resolution codes are in a very good agreement. The parameterization errors generally do not exceed 20% of deviation everywhere except mesospheric J_{O2} and J_{H2O}. Comparison of this experiment results with Figure 7 shows that schemes with clear problems in representation of the absolute values can still reproduce well the solar variability-induced changes (e.g., SUNY-SPB and HP stratospheric J_{O2}), and the other way around, schemes with a good representation of the absolute values can suffer in terms of variability representation (e.g., SOCOL and Fast-JX-UKCA mesospheric J_{O2}).

Using RCPM we then analyzed the effects caused by the obtained deviations. We applied the solar signal in J_{O2}, J_{O3}, and J_{H2O} calculated by each of the codes as correction factors to RCPM photolysis profiles. The difference between each of the codes and libRadtran results (Figure 4, JR COSI-full case) is shown in Figure 10. In the stratosphere, the representation of the solar signal due to photolysis rates is rather good and differs between parameterizations within ±0.3% for ozone and ±0.05 K for temperature. In the mesosphere, the difference is much larger—by up to 6% in ozone and 0.7 K in temperature, mainly due to the response of J_{O2} and J_{H2O} to the SSI enhancement. The apparent outlier is the SOCOL scheme in the lower mesosphere. The SPARC CCMVal multiple linear regression analysis of a number of observational and modeled data sets showed that only the SOCOL CCM reveals negative solar regression coefficients in the lower mesospheric ozone [*SPARC CCMVal report*, 2010], which can be potentially attributed to the overestimated J_{H2O} response to SSI in SOCOL presented in our study, since the SOCOL heating rates changes representation was shown to be good in this region [*Forster et al*., 2011]. We highlight that the effects presented are related only to the photolysis changes and they can be compensated or enhanced by the feedback with heating rates, whose representation can also significantly suffer in CCMs [*Forster et al*., 2011], as well as by dynamical feedbacks.

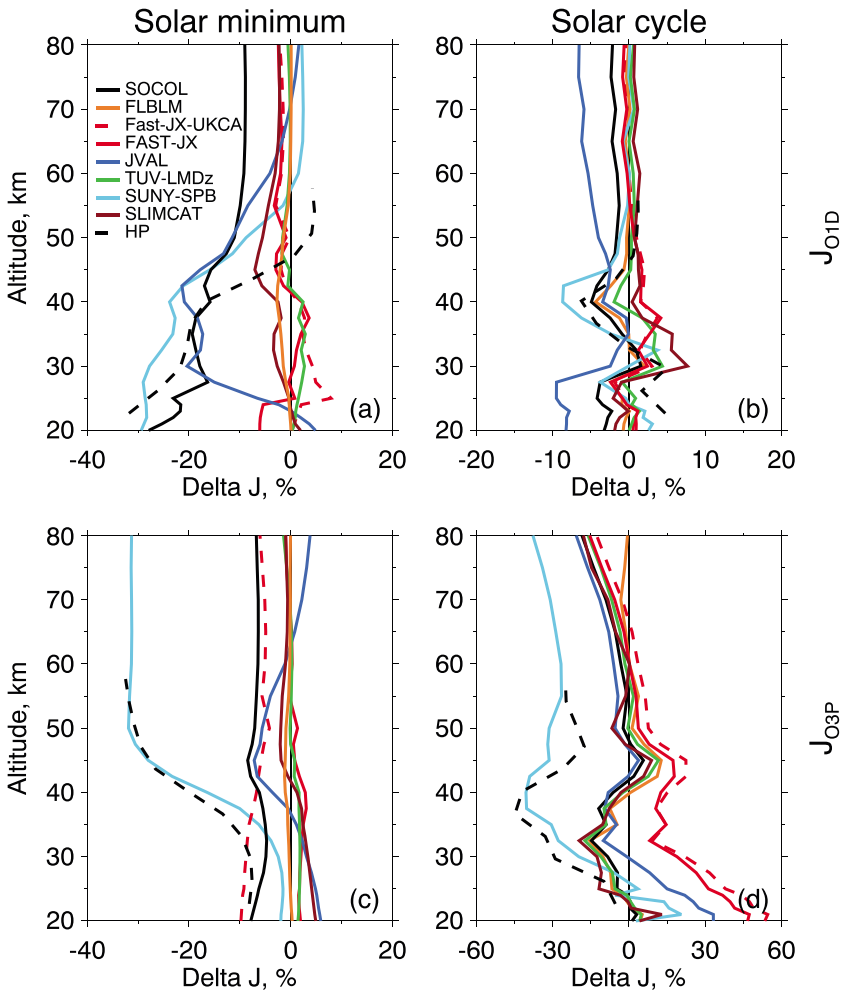

Figure 11. Same as in Figures 7a and 7d and Figures 9c and 9f but for (a, b) J_{O1D} and (c, d)J_{O3P}.

5.4. J_{O3P} and J_{O1D} Uncertainty

Special attention needs to be paid to the representation of J_{O3P} and J_{O1D} by parameterizations. Figure 11 shows the same differences to libRadtran as in Figures 7 and 9 but for J_{O1D} and J_{O3P}. Compared to the total ozone photolysis case ($J_{O1D} + J_{O3P}$) the J_{O1D} results from SOCOL, SUNY-SPB, JVAL, and HP are quite different, while the results of TUV-LMDz, Fast-JX, Fast-JX-UKCA, and SLIMCAT remain nearly the same. The difference between J_{O3P} and J_{O1D} deviations can be partly attributed to the treatment of the quantum yields, which are strongly temperature and wavelength dependent [*Sander et al.*, 2011]. Besides this, it can be related to the parameterizations' problems in representing the propagation of longer or shorter wavelengths. Thus, the treatment of Rayleigh scattering, which is more important for shorter wavelengths and lower altitudes, can be another reason for the J_{O1D} underestimation of SOCOL, HP, and SUNY-SPB schemes, in particular because these three schemes show similar behavior for HNO_3 and Cl_2O_2, which also absorb in the middle UV. In contrast, their representation of J_{O3P} in the lower stratosphere, which is dominated by the Chappius bands, does not exceed ±10% deviation range.

6. Summary and Conclusions

To evaluate the uncertainty in modeling studies investigating the Sun-Earth interactions, we analyzed effects of two primary sources of uncertainty—SSI variability and photolysis rate parameterizations. First, we performed sensitivity experiments with a 1-D model (RCPM) and showed that the most important photodissociation reactions for tropical ozone in the stratosphere and mesosphere are the photolysis of oxygen and

ozone and water vapor in the mesosphere. The ozone sensitivity to photolysis of other species is much lower compared to these species. Further, using the high-resolution libRadtran model and different SSI data sets (COSI and NRL reconstructions and SORCE observations), we calculated the solar signal in photolysis rates of these three species and of three other species which photodissociate in different spectral intervals (HNO_3, Cl_2O_2, and NO_2). Additional experiments with RCPM revealed the high impact of the spectral variations between SSI data sets on the middle atmospheric ozone and temperature. As oxygen and ozone photolysis effects can compensate each other, the more important parameter for ozone becomes not the magnitude of SSI variations but the ratio between the SSI variations in the 175–242 nm (oxygen photolysis) and 242–350 nm (ozone photolysis) intervals. We showed that because of this, the differences between RCPM calculations forced by the SORCE SSI data set and COSI or NRL SSI data sets can be of similar magnitude as the differences between RCPM calculations forced by COSI and NRL data sets. However, for the solar signal in temperature, the absolute SSI changes in both spectral intervals are the important quantities, since both absorption of oxygen and ozone contribute to an increase in heating rates.

A number of studies have exploited general circulation models (GCMs) to investigate the solar effects in the atmosphere using fixed climatological ozone or ozone with the solar component derived from the observational data sets using multilinear regression techniques (MLR) [e.g., *Ineson et al*., 2011; *Hood et al*., 2013; *Ineson et al*., 2015; *Maycock et al*., 2015]. If a study excludes the ozone feedback, our results suggest that it can miss up to half of the stratospheric temperature response with nonlinear implications for the surface response. Several GCM studies [e.g., *Haigh*, 1999; *Hood et al*., 2013] have shown a high sensitivity of results to the applied latitudinal and altitudinal distributions of the stratospheric ozone due to the solar cycle variations. *Chiodo et al*. [2014] showed that the proper MLR derivation of such distributions is problematic due to contamination of the observational time series by volcanic eruptions. Another disadvantage of MLR-derived solar signal in ozone is the scaling of ozone changes to the total solar irradiance or integrated UV flux in order to account for the solar forcing, while the spectral features are shown to affect differently the shape of the ozone vertical changes.

Evaluation of the performances of eight state-of-the-art CCM photolysis parameterizations in terms of middle atmosphere climatology and solar signal demonstrated that, in most cases, results from different parameterizations agree within 30%. However, each scheme shows large deviations from the reference schemes caused by specific reasons including Rayleigh scattering, quantum yields, and absorption cross-sections treatments. The largest effect of parameterization uncertainty is found in the mesosphere and is related to the treatment of the Lyman alpha line and Schumann-Runge bands, both for the solar signal and for the state of the atmosphere during the solar minimum. A 1-D modeling analysis of the parameterization spread revealed that the quality of the parameterizations has a strong influence on the climatological state of global models, which implement these parameterizations, as well as on their representation of solar signal.

Our results highlight the necessity of obtaining proper SSI variations as well as accurate photolysis rate calculations in chemistry-climate modeling. We show that some parameterizations implemented in global 3-D models are already good enough to simulate the main photodissociation processes driving the middle atmospheric response to solar variations, i.e., the J_{O2}, J_{O3}, and J_{H2O} changes. Features of other parameterizations presented in our study are useful to take into account for the analysis of global modeling results.

Acknowledgments

This research was funded in part by the Swiss National Science Foundation under grant agreements 200020_140573, 200020_153302, 200021_149182 (SILA), CRSI22_130642 (FUPSOL), CRSII2_147659 (FUPSOL II). Fruitful discussions with the COST Action ES1005 TOSCA (http://www.tosca-cost.eu) community are much appreciated. Alexander Shapiro acknowledges support through the People Programme (Marie Curie Actions) of the European Union's Seventh Framework Programme (FP7/2007–2013) under REA grant agreement 624817. The work of Sergei Smyshlyaev was supported by the Russian Foundation for Basic Research (project 14-05-00871) and Russian Scientific Foundation (project 14-17-00096). The SLIMCAT/TOMCAT modeling work was supported by NERC through the MAPLE project (NE/J008621/1) and NCAS. The work of Boris Fomin was supported by Russian Foundation for Basic Research (grants 15-01-00783 and 14-01-00197). The work of Sebastien Bossay, Slimane Bekki, and Marion Marchand was supported by the grant "SOLSPEC" from the Centre d'Etude Spatiale (CNES) and by the European project StratoClim (seventh framework program, grant agreement 603557). We thank Michael Prather for the provision of the Fast-JX code and fruitful discussions. We acknowledge NRL SSI data from http://lasp.colorado.edu/lisird/ and SORCE data from http://lasp.colorado.edu/home. COSI SSI data are available on request.

References

Atkinson, R., D. L. Baulch, R. A. Cox, J. N. Crowley, R. F. Hampson, R. G. Hynes, M. E. Jenkin, M. J. Rossi, and J. Troe (2004), IUPAC Task Group on atmospheric chemical kinetic data evaluation, *Atmos. Chem. Phys.*, *4*, 1461–1738. [Available at http://iupac.pole-ether.fr.]

Ball, W. T., N. A. Krivova, Y. C. Unruh, J. D. Haigh, and S. K. Solanki (2014), A new SATIRE-S spectral solar irradiance reconstruction for solar cycles 21–23 and its implications for stratospheric ozone, *J. Atmos. Sci.*, *71*, 4086–4101, doi:10.1175/JAS-D-13-0241.1.

Ball, W. T., J. D. Haigh, E. V. Rozanov, A. Kuchar, T. Sukhodolov, F. Tummon, and A. V. Shapiro (2016), High solar cycle spectral variations inconsistent with stratospheric ozone observations, *Nat. Geosci.*, doi:10.1038/ngeo2640M3.

Bian, H. S., and M. J. Prather (2002), Fast-J2: Accurate simulation of stratospheric photolysis in global chemical models, *J. Atmos. Chem.*, *41*, 281–296.

Brasseur, G. P., and P. C. Simon (1981), Stratospheric chemical and thermal response to long-term variability in solar UV irradiance, *J. Geophys. Res.*, *86*, 7343–7362, doi:10.1029/JC086iC08p07343.

Brasseur, G. P., and S. Solomon (2005), *Aeronomy of the Middle Atmosphere*, 658 pp., Springer, New York.

Chiodo, G., D. R. Marsh, R. Garcia-Herrera, N. Calvo, and J. A. García (2014), On the detection of the solar signal in the tropical stratosphere, *Atmos. Chem. Phys. Discuss.*, *13*, 30,097–30,142, doi:10.5194/acpd-13-30097-2013.

Chipperfield, M. P., W. Feng, and M. Rex (2005), Arctic ozone loss and climate sensitivity: Updated three-dimensional model study, *Geophys. Res. Lett.*, *32*, L11813, doi:10.1029/2005GL022674.

Dhomse, S., M. P. Chipperfield, W. Feng, and J. D. Haigh (2011), Solar response in tropical stratospheric ozone: A 3-D chemical transport model study using ERA reanalyses, *Atmos. Chem. Phys.*, *11*, 12,773–12,786, doi:10.5194/acp-11-12773-2011.

Dvortsov, V. L., S. G. Zvenigorodsky, and S. P. Smyshlyaev (1992), On the use of Isaksen-Luther method of computing photodissociation rates in photochemical models, *J. Geophys. Res.*, *97*, 7593–7601, doi:10.1029/91JD02861.

Egorova, T., I. Karol, and E. Rozanov (1997), The influence of ozone content loss in the lower stratosphere on the radiative balance of the troposphere, *Phys. Atmos. Ocean (Russ. Acad. Sci.)*, *33*, 492–499.

Egorova, T., E. Rozanov, E. Manzini, M. Haberreiter, W. Schmutz, V. Zubov, and T. Peter (2004), Chemical and dynamical response to the 11-year variability of the solar irradiance simulated with a chemistry-climate model, *Geophys. Res. Lett.*, *31*, L06119, doi:10.1029/2003GL019294.

Ermolli, I., et al. (2013), Recent variability of the solar spectral irradiance and its impact on climate modelling, *Atmos. Chem. Phys.*, *13*, 3945–3977, doi:10.5194/acp-13-3945-2013.

Fomin, B., and V. Falaleeva (2012), A polarized atmospheric radiative transfer model for calculations of spectra of the stokes parameters of shortwave radiation based on the line-by-line and Monte Carlo methods, *Atmosphere*, *3*, 451–467, doi:10.3390/atmos3040451.

Forster, P. M., et al. (2011), Evaluation of radiation scheme performance within chemistry climate models, *J. Geophys. Res.*, *116*, D10302, doi:10.1029/2010JD015361.

Gray, L. J., et al. (2010), Solar influences on climate, *Rev. Geophys.*, *48*, RG4001, doi:10.1029/2009RG000282.

Haigh, J. D. (1994), The role of stratospheric ozone in modulating the solar radiative forcing of climate, *Nature*, *370*, 544–546, doi:10.1038/370544a0.

Haigh, J. D. (1996), The impact of solar variability on climate, *Science*, *272*, 981–984.

Haigh, J. D. (1999), A GCM study of climate change in response to the 11-year solar cycle, *Q. J. R. Meteorol. Soc.*, *125*, 871–892.

Haigh, J. D., A. R. Winning, R. Toumi, and J. W. Harder (2010), An influence of solar spectral variations on radiative forcing of climate, *Nature*, *467*, 696–699, doi:10.1038/nature09426.

Harder, J. W., J. M. Fontenla, P. Pilewskie, E. C. Richard, and T. N. Woods (2009), Trends in solar spectral irradiance variability in the visible and infrared, *Geophys. Res. Lett.*, *36*, L07801, doi:10.1029/2008GL036797.

Harwood, R. S., and J. A. Pyle (1975), A two-dimensional mean circulation model for the atmosphere below 80 km, *Q. J. R. Meteorol. Soc.*, *101*, 723–747, doi:10.1002/qj.49710143003.

Hood, L., S. Schimanke, T. Spangehl, S. Bal, and U. Cubasch (2013), The surface climate response to 11-yr solar forcing during northern winter: Observational analyses and comparisons with GCM simulations, *J. Clim.*, *26*, 7489–7506.

Hsu, J., M. J. Prather, D. Bergmann, and P. Cameron-Smith (2013), Sensitivity of stratospheric dynamics to uncertainty in O_3 production, *J. Geophys. Res. Atmos.*, *118*, 8984–8999, doi:10.1002/jgrd.50689.

Ineson, S., A. Scaife, J. R. Knight, J. C. Manners, N. J. Dunstone, L. J. Gray, and J. D. Haigh (2011), Solar forcing of winter climate variability in the Northern Hemisphere, *Nat. Geosci.*, *4*, 753–757.

Ineson, S., A. C. Maycock, L. J. Gray, A. A. Scaife, N. Dunstone, J. Harder, J. R. Knight, M. Lockwood, J. C. Manners, and R. Wood (2015), Regional climate impacts of a possible future grand solar minimum, *Nat. Commun.*, *6*, 7535, doi:10.1038/ncomms8535.

Isaksen, I. S. A., K. H. Midtbo, J. Sunde, and P. J. Crutzen (1977), A simplified method to include molecular scattering and reflection in calculations of photon fluxes and photodissociation rates, *Geophys. Norv.*, *31*, 11.

Kidston, J., A. A. Scaife, S. C. Hardiman, D. M. Mitchell, N. Butchart, M. P. Baldwin, and L. J. Gray (2015), Stratospheric influence on tropospheric jet streams, storm tracks and surface weather, *Nat. Geosci.*, *8*, 433–440, doi:10.1038/ngeo2424.

Kodera, K., and Y. Kuroda (2002), Dynamical response to the solar cycle, *J. Geophys. Res.*, *107*(D24), 4749, doi:10.1029/2002JD002224.

Kurucz, R. (1993), *ATLAS9 Stellar Atmosphere Programs and 2 km/s Grid*, *Kurucz CD-ROM No. 13*, Smithsonian Astrophys. Obs., Cambridge, Mass.

Landgraf, J., and P. J. Crutzen (1998), An efficient method for online calculations of photolysis and heating rates, *J. Atmos. Sci.*, *55*, 863–878.

Lary, D. J., and J. A. Pyle (1991), Diffuse radiation, twilight and photochemistry, *J. Atmos. Chem.*, *13*, 373–392.

Lean, J. (1997), The Sun's variable radiation and its relevance for Earth, *Annu. Rev. Astron. Astrophys.*, *35*, 33–67, doi:10.1146/annurev.astro.35.1.33.

Lean, J. L. (2000), Evolution of the Sun's spectral irradiance since the Maunder Minimum, *Geophys. Res. Lett.*, *27*, 2425–2428, doi:10.1029/2000GL000043.

Madronich, S., and S. Flocke (1999), The role of solar radiation in atmospheric chemistry, in *Handbook of Environmental Chemistry*, edited by P. Boule, pp. 1–26, Springer, Berlin.

Marchand, M., et al. (2012), Dynamical amplification of the stratospheric solar response simulated with the chemistry-climate model LMDz-Reprobus, *J. Atmos. Sol. Terr. Phys.*, *75-76*, 147–160.

Maycock, A. C., S. Ineson, L. J. Gray, A. A. Scaife, J. A. Anstey, M. Lockwood, N. Butchart, S. C. Hardiman, D. M. Mitchell, and S. M. Osprey (2015), Possible impacts of a future Grand Solar Minimum on climate: Stratospheric and global circulation changes, *J. Geophys. Res. Atmos.*, *120*, 9043–9058, doi:10.1002/2014JD022022.

Mayer, B., and A. Kylling (2005), Technical note: The libradtran software package for radiative transfer calculations–description and examples of use, *Atmos. Chem. Phys.*, *5*, 1855–1877, doi:10.5194/acp-5-1855-2005.

McClatchey, R. A., R. W. Fenn, J. E. A. Selby, F. E. Volz, and J. S. Garing (1972), *Optical Properties of Atmosphere*, *AFCRL-72-0497*, 3rd ed., Environmental Research Papers, *411*, Massachusetts.

Mlynczak, M. G., and S. Solomon (1993), A detailed evaluation of the heating efficiency in the middle atmosphere, *J. Geophys. Res.*, *98*, 10,517–10,541, doi:10.1029/93JD00315.

Molina, L. T., and M. J. Molina (1986), Absolute absorption cross sections of ozone in the 185- to 350-nm wavelength range, *J. Geophys. Res.*, *91*, 14,501–14,508, doi:10.1029/JD091iD13p14501.

Molina, L. T., and M. J. Molina (1987), Production of Cl_2O_2 from the self-reaction of the ClO radical, *J. Phys. Chem.*, *91*(2), 433–436.

Nicolet, M. (1985), Aeronomical aspects of mesospheric photodissociation: Processes resulting from the solar H Lyman-alpha line, *Planet. Space Sci.*, *33*, 69–80.

Nissen, K. M., K. Matthes, U. Langematz, and B. Mayer (2007), Towards a better representation of the solar cycle in general circulation models, *Atmos. Chem. Phys.*, *7*, 5391–5400, doi:10.5194/acp-7-5391-2007.

Oberländer, S., U. Langematz, K. Matthes, M. Kunze, A. Kubin, J. Harder, N. A. Krivova, S. K. Solanki, J. Pagaran, and M. Weber (2012), The influence of spectral solar irradiance data on stratospheric heating rates during the 11 year solar cycle, *Geophys. Res. Lett.*, *39*, L01801, doi:10.1029/2011GL049539.

Olson, J., et al. (1997), Results from the Intergovernmental Panel on Climatic Change Photochemical Model Intercomparison (PHOTOCOMP), *J. Geophys. Res.*, *102*, 5979–5991, doi:10.1029/96JD03380.

Prather, M. J. (2015), Photolysis rates in correlated overlapping cloud fields: Cloud-J 7.3c, *Geosci. Model Dev.*, *8*, 2587–2595, doi:10.5194/gmd-8-2587-2015.

Rozanov, E., M. E. Schlesinger, V. Zubov, F. Yang, and N. G. Andronova (1999), The UIUC three-dimensional stratospheric chemical transport model: Description and evaluation of the simulated source gases and ozone, *J. Geophys. Res.*, *104*, 11,755–11,781, doi:10.1029/1999JD900138.

Rozanov, E., T. Egorova, C. Fröhlich, M. Haberreiter, T. Peter, and W. Schmutz (2002), Estimation of the ozone and temperature sensitivity to the variation of spectral solar flux, in *Proceedings of the SOHO11 Symposium: "From Solar Min to Max: Half a Solar Cycle With SOHO"*, *ESASP-508*, edited by A. Wilson, pp. 181–184, ESA SP-508, pp. 223–226, ESA Publications Division, Noordwijk, Netherlands.

Rozanov, E., T. Egorova, W. Schmutz, and T. Peter (2006), Simulation of the stratospheric ozone and temperature response to the solar irradiance variability during Sun rotational cycle, *J. Atmos. Sol. Terr. Phys.*, *68*, 2203–2213.

Sander, R., P. Jöckel, O. Kirner, A. T. Kunert, J. Landgraf, and A. Pozzer (2014), The photolysis module JVAL-14, compatible with the MESSy standard, and the JVal PreProcessor (JVPP), *Geosci. Model Dev.*, *7*, 2653–2662, doi:10.5194/gmd-7-2653-2014.

Sander, S. P., et al. (2006), *Chemical Kinetics and Photochemical Data for Use in Atmospheric Studies*, *Eval. Number 15, Tech. Rep.*, NASA JPL, Pasadena, Calif. [Available at http://jpldataeval.jpl.nasa.gov.]

Sander, S. P., et al. (2011), *Chemical Kinetics and Photochemical Data for Use in Atmospheric Studies*, *Eval. No. 17, JPL Publ. 10-6*, Jet Propul. Lab., Pasadena, Calif. [Available at http://jpldataeval.jpl.nasa.gov.]

Shapiro, A. I., W. Schmutz, M. Schoell, M. Haberreiter, and E. Rozanov (2010), NLTE solar irradiance modeling with the COSI code, *Astron. Astrophys.*, *517*, A48, doi:10.1051/0004-6361/200913987.

Shapiro, A. I., W. Schmutz, E. Rozanov, M. Schoell, M. Haberreiter, A. V. Shapiro, and S. Nyeki (2011), A new approach to the long-term reconstruction of the solar irradiance leads to large historical solar forcing, *Astron. Astrophys.*, *529*, A67, doi:10.1051/0004-6361/201016173.

Shapiro, A. V., E. Rozanov, A. I. Shapiro, S. Wang, T. Egorova, W. Schmutz, and T. Peter (2012), Signature of the 27-day solar rotation cycle in mesospheric OH and H_2O observed by the Aura Microwave Limb Sounder, *Atmos. Chem. Phys.*, *12*, 3181–3188, doi:10.5194/acp-12-3181-2012.

Shapiro, A. V., E. V. Rozanov, A. I. Shapiro, T. A. Egorova, J. Harderi, M. Weber, A. K. Smith, W. Schmutz, and T. Peter (2013), The role of the solar irradiance variability in the evolution of the middle atmosphere during 2004–2009, *J. Geophys. Res. Atmos.*, *118*, 3781–3793, doi:10.1002/jgrd.50208.

Smyshlyaev, S. P., V. L. Dvortsov, M. A. Geller, and V. A. Yudin (1998), A two dimensional model with input parameters from a GCM: Ozone sensitivity to different formulation for the longitudinal temperature variation, *J. Geophys. Res.*, *103*, 28,373–28,387, doi:10.1029/98JD02354.

Solanki, S. K., and Y. C. Unruh (1998), A model of the wavelength dependence of solar irradiance variations, *Astron. Astrophys.*, *329*, 747–753.

Solanki, S. K., N. A. Krivova, and J. D. Haigh (2013), Solar irradiance variability and climate, *Annu. Rev. Astron. Astrophys.*, *51*, 311–351, doi:10.1146/annurev-astro-082812-141007.

SPARC CCMVal (2010), *SPARC Report on the Evaluation of Chemistry-Climate Models*, *SPARC Rep. 5*, edited by V. Eyring, T. G. Shepherd, and D. W. Waugh, Univ. of Toronto, Toronto, Ont., Canada. [Available at http://www.atmosp.physics.utoronto.ca/SPARC.]

Stenke, A., M. Schraner, E. Rozanov, T. Egorova, B. Luo, and T. Peter (2013), The SOCOL version 3.0 chemistry-climate model: Description, evaluation, and implications from an advanced transport algorithm, *Geosci. Model Dev.*, *6*, 1407–1427, doi:10.5194/gmd-6-1407-2013.

Swartz, W. H., R. S. Stolarski, L. D. Oman, E. L. Fleming, and C. H. Jackman (2013), Middle atmosphere response to different descriptions of the 11-yr solar cycle in spectral irradiance in a chemistry-climate model, *Atmos. Chem. Phys.*, *12*, 5937–5948, doi:10.5194/acp-12-5937-2012.

Talukdar, R. K., C. A. Longfellow, M. K. Gilles, and A. R. Ravishankara (1998), Quantum yields of $O(^1D)$ in the photolysis of ozone between 289 and 329 nm as a function of temperature, *Geophys. Res. Lett.*, *25*, 143–146, doi:10.1029/97GL03354.

Telford, P. J., N. L. Abraham, A. T. Archibald, P. Braesicke, M. Dalvi, O. Morgenstern, F. M. O'Connor, N. A. D. Richards, and J. A. Pyle (2013), Implementation of the Fast-JX Photolysis scheme (v6.4) into the UKCA component of the MetUM chemistry-climate model (v7.3), *Geosci. Model Dev.*, *6*, 161–177, doi:10.5194/gmd-6-161-2013.

Thuillier, G., et al. (2014a), The solar irradiance spectrum at solar activity minimum between solar cycles 23 and 24, *Sol. Phys.*, *289*(6), 1931–1958, doi:10.1007/s11207-013-0461-y.

Thuillier, G., S. M. L. Melo, J. Lean, N. A. Krivova, C. Bolduc, V. I. Fomichev, P. Charbonneau, A. I. Shapiro, W. Schmutz, and D. Bolsée (2014b), Analysis of different solar spectral irradiance reconstructions and their impact on solar heating rates, *Sol. Phys.*, *289*(4), 1115–1142, doi:10.1007/s11207-013-0381-x.

Thuillier, G., J. W. Harder, A. Shapiro, T. N. Woods, J.-M. Perrin, M. Snow, T. Sukhodolov, and W. Schmutz (2015), The infrared solar spectrum measured by the SOLSPEC spectrometer onboard the International Space Station, *Sol. Phys.*, *290*, 1581–1600, doi:10.1007/s11207-015-0704-1.

von Hobe, M., et al. (2007), Understanding the kinetics of the ClO dimer cycle, *Atmos. Chem. Phys.*, *7*, 3055–3069.

Wild, O., X. Zhu, and M. J. Prather (2000), Fast-J: Accurate simulation of in- and below-cloud photolysis in tropospheric chemical models, *J. Atmos. Chem.*, *37*, 245–282.

Zhong, W., S. M. Osprey, L. J. Gray, and J. D. Haigh (2008), Influence of the prescribed solar spectrum on calculations of atmospheric temperature, *Geophys. Res. Lett.*, *35*, L22813, doi:10.1029/2008GL035993.